WASP-2b
Exoplanet Confirmation and Radius Calculation

By: Anika Nath

12.410 Final Project Report

11/12/2023

Abstract

The transit of WASP-2b was observed and analyzed to confirm the existence of the exoplanet, and to determine the transit depth and radius of WASP-2b. One full transit of WASP-2b was observed at the Wallace Astrophysical Observatory through a 14-inch Celestron telescope on October 24, 2023 just after midnight [UTC]. The data were collected and then analyzed to get the result. The study confirmed the existence of the planet, and detected its ingress with a 99% confidence level. A transit depth of 11.9 ± 0.4 ppt was calculated, which is 12.9% of the predicted value which is 91.6 ppt. From this transit depth, the radius of WASP-2b was calculated to be 0.886 ± 0.014 R_{Jup}. The radius was lower than the previous result of 1.04 ± 0.06 R_{Jup} found by A. Collier Cameron et al., 2007. The difference here is likely due to the poor quality of data collected during the study and the presence of clouds in the atmosphere during the transit. However, the error in my calculations was low because it was calculated using the standard deviation of the mean, instead of the sample standard deviation. The radius calculations in this study are inclusive, and it is recommended that future work should collect data from several transits under good atmospheric conditions to calculate a more accurate value of the radius of WASP-2b.

Background

There are more than 5,000 known exoplanets, and thousands more waiting to be found (Fujii, Y. et al., 2018). There are multiple methods to detect exoplanets, like transit, direct imaging, astrometry, radial velocity and gravitational microlensing (Wright, J.T. and Gaudi, B.S., 2012). This paper focuses on the transit method, which works by detecting a dip in the star’s brightness from the planet when it blocks a fraction of the star’s light every time the planet crosses the star. In 1999, the first exoplanet was observed with this technique (David Charbonneau et al. 2000). Since then, this method has been used to discover several thousand exoplanets (Perryman, 2011).

The transit method works well with a higher ratio of the planet radius to the star's radius because then the planet will block more light during transits, which will make the dip easier to detect (Wright, J.T. and Gaudi, B.S. 2012). This includes hot Jupiters, which are Jupiter-mass planets at a distance of less than 0.1 A.U. from their host stars, and have typical orbital periods of only a few days (Jonathan J. Fortney et al. 2021). Since they are relatively massive and have shorter orbits (leading to more frequent transits), the signal to noise ratio is higher during observation. This is what makes them easier to detect than some other types of planets (Perryman, 2011).

Figure 1: Transit Light Curve for the Hot Gas Giant Exoplanet WASP-96b. As the planet passes in front of its parent star, there is a dip in the star's relative brightness as a portion of the starlight is blocked by the planet. (Exoplanet Exploration 2022.)

An increasing number of exoplanets are being discovered by capturing transits through wide-angle searches. These searches use telescopes that are equipped with specialized instruments (like lenses and cameras) to capture a large portion of the sky at one time. The WASP (Wide-Angle Search for Planets) project is designed to search for exoplanets using the transit method. It includes a network of wide-angle, ground-based telescopes in order to look at large areas of the night sky. There are 2 wide-field camera arrays: one in La Palma, Canary Islands (Spain) and the other one in Sutherland, South Africa (Perryman, 2011).

The SuperWASP project builds on the WASP project to provide more comprehensive and detailed observations for exoplanet searches. It conducts all-sky surveys, much broader than those done by WASP. Using SuperWASP, one exoplanet is confirmed per 5-6 exoplanets selected for radial velocity follow-up using SOPHIE, a high-resolution spectrograph (Ignatov et al., 2020).

The SuperWASP observing session during 2004 May–September resulted in a set of exoplanet candidates (A. Collier Cameron et al., 2007). One candidate was the star WASP-2 located about 470 light years away in the constellation of Delphinus, with a radius of 580,000 km (Universe Guide, 2023).

WASP-2b was detected by the SuperWASP-North telescope and the Wide Angle Search for

Planets (WASP) project (A. Collier Cameron et al., 2007). WASP-2b lies between hot Jupiters and very hot Jupiters. The initial observations found the WASP-2b radius to be in the range 0.65–1.26 R_{Jup} (A. Collier Cameron et al., 2007). A future study (by Charbonneau et al., 2007) determined the radius of WASP-2b to be 1.04 ± 0.06 R_{Jup}.

This study aims to provide an independent confirmation of the existence of the exoplanet WASP-2b, using the transit method as it passes in front of its star, WASP-2. Further, it aims to use the depth of the light curve and the radius of the host star to calculate the radius of the exoplanet.

Figure 2 (Ignatov, 2020) shows that the relative flux of the star, WASP-2, drops approximately 0.26% due to the transit of WASP-2b. In the legend, WASP-2 is labeled as “object”, and the comparison star, GCS 0052201406, is labeled as “check star". The flux of the check star remains fairly constant during the entire observation time.

Observations and Calibration

During September and October 2023, data were gathered successfully during 3 different observation sessions at the Wallace Observatory in Westford, MA, with each session lasting about 4 hours. The exoplanets studied during these sessions were WASP-2b and WASP-26b. These objects were chosen because they start appearing during the beginning of the observing time (about 01:00 UTC), and disappear during the end of our observing time (about 03:00 UTC). Also, the depth of the light curve (from the point at which the planet is not transiting the

star to the middle if the transit) is more than 10 ppt, so the transit should be observable above the noise.

Details of the observations are illustrated in Table 1:

Table 1: Summary of Equipment and location

Date (UTC)	Observation object	Location	Filter	Equipment used	Conditions and Observations
2023-09-26 00:20-03:20	WASP-2b	Pier 1	Clear filter	14-inch Celestron	The weather was cloudy.
2023-10-03 00:24-03:34	WASP-26b	Pier 2	Clear filter	14-inch Celestron	Transit was not observed.
2023-10-24 00:22-04:00	WASP-2b	Pier 2	Clear filter	14-inch Celestron	Transit was clearly observed.

Note: *A clear filter was used because it has a larger bandwidth, so more light could get in. Therefore, the signal-to-noise ratio (SNR) was higher compared to the SNR from a narrow bandwidth filter. Further, the goal of the study did not include focusing on specific wavelengths to detect gasses.*

The data from the session on 2023-09-26 was not used in the final study since it was cloudy during the time when data were collected. The data from the session on 2023-10-03 was not used in the final study since the transit was not clearly observed during the time data were collected, as shown in Figure 3.

Figure 3: Initial Relative flux of WASP-26 over the entire observation period. Note that the flux remains constant until 2.5 UTC, and then dips slightly around 2.75 UTC. It reaches a maximum point at 3.0 UTC. However, the transit is not clearly observed, so I will disregard this data for the rest of the analyses.

Observational Times	Session Details	Images Taken	Exposure Duration	Rationale & Analysis
00:22- 00:34	Pointed the telescope at the object, and focused the images	N/A	N/A	Ensured that the object was located near the center of the frame and that it was clearly visible
00:34- 03:50	Captured Images	122 Science Images	90 seconds	90 second exposure duration helped with the sharpest images. Images captured with an exposure duration less than 90 seconds resulted in images that were not clear since the target star was not bright enough. Images captured with an exposure duration less than 90 seconds resulted in oversaturation.
03:50- 03:58	Captured Images	5 Dark Images	90 seconds	90 second exposure duration matched the exposure duration of science images.
03:58- 04:00	Captured Images	20 Bias Images	N/A	

Transit was clearly observed on 2023-10-24, and data collected during this session is used for the rest of this study. The celestial coordinates for the entire observing session was right ascension = 19:34:55.87 and declination = +36:48:55.78. Also, the telescope was at -10 C rather than usual -20 C in order to prevent the CCD window from icing over due to extreme humidity at the site. Details of each part of this observation session are illustrated in Table 2:

Table 2: Summary of Data Collected on 2023-10-24. Transit of WASP-2b was observed from the 14-inch Celestron telescope on Pier 2 using clear filter

Calibrations were performed on the main images of the target star using the AstroImageJ software. For the calibrations, the software reduced the primary science images by compensating for biases, darks and flats in order to determine the signal by accounting for systematic uncertainties. The biases account for the uncertainty of the voltage of each pixel in the CCD, so that when the voltage is converted to a number, it is always positive. The dark image accounts for the dark current, which is caused by the thermal effects in the CCD. The flat images account for non-uniform illumination of the CCD.

Dark images were captured using the 90 seconds exposure time duration, matching the capture duration of the science images. These dark images were then combined to create a master dark file, shown in Figure 4, in order to reduce the noise variation in each dark file.

Figure 4: Master dark file used during calibration to compensate for effects of dark currents and hot pixels that are caused by the thermal effects in the CCD.

Flats were captured using the same clear filter to match the filter used to capture the science images. Figure 5 shows the master flat file used during calibration (Dr Person, Course 12 staff, 2023).

Figure 5: Master flat file used during calibration to compensate for the CCD's not being illuminated uniformly.

Bias images were captured at the same CCD temperature as science images, and combined to create the master bias, which was then subtracted from the science images to account for the offset caused by the electronics. Figure 6 shows the master bias file used during calibration.

Figure 6: Master bias file used during calibration to compensate for offset caused by electronics.

Calibrated science images were obtained after reducing them using the master bias, dark and flat files. An example of unreduced and reduced images is shown in Figure 7.

a) Unreduced Science Image b) Reduced Science Image

Figure 7: Unreduced and reduced science images. The image in part (a) shows one of the original science images, and the image in part (b) shows the corresponding calibrated image. In both images, the target star is circled in blue.

Multi-aperture photometry was performed to get the light curve of the transit star. This was done to remove any variation in brightness that occurred over the period in which images were captured due to sources such as the atmosphere.

For this, 5 stars were selected as comparison stars for the target star. This was done by relying on the visual brightness of the stars to choose ones that had similar brightness to the target star. I also made sure that the variable stars had a constant brightness (see Figure 14). Proximity to

the target star was also considered to select the comparison stars, and caution was also taken to ensure these comparison stars were not near the edges of the image in order to ensure that they were observed under the same atmospheric conditions as the target star. The target star and the comparison stars are shown in Figure 8.

Figure 8: Target star and comparison stars. In the figure, the target star is circled in blue, and the comparison stars are circled in magenta. The comparison stars are similar in brightness to the target star, and used to measure the brightness of the target star. Note that the comparison stars surround the target star to sample the main portion of the sky.

For capturing the images of the target star as well as the 5 comparison stars, an aperture radius of 6 pixels was used, based on the width of the widest star used (leftmost star in Figure 8). In order to calculate the relative flux of a single star, AstroImageJ first calculates the relative photoelectric count from the source and background by using a small aperture for the star, as shown as the source box in Figure 9. Then it uses a larger aperture to calculate the photoelectric count from the background itself, as shown as the background box in Figure 10. The relative flux of a single star is calculated by subtracting the photoelectric count from the background itself by the photoelectric count from the source and background.

Figure 9: Shows how the ADU varies as the aperture size increases for a single star. ADU here stands for Analog Data Unit, and represents the number of photoelectrons divided by the gain. The ADU for the source part represents the photoelectric count from the source and background. The ADU for the background part represents the photoelectric count from the background itself. The relative flux of a single star is calculated by subtracting the photoelectric count from the background itself by the photoelectric count from the source and background.

Theses calibrations resulted in the reduced images showed in parts (c) and (d) of Figure 10

Computations

Data Validation

The collected data were first evaluated to filter out any possible outliers. The relative flux of WASP-2 was plotted for all points in the observation period, as shown in Figure 11.

Figure 10: Initial Relative flux of WASP-2 over the entire observation period with the two points that have maximum flux as possible outliers.

A hypothesis test was performed to reject possible outliers, which are the two points with the highest flux that are seen in Table 3. For each t-test, the t value was calculated based on Equation 1, which is written as

Equation 1: t = abs((flux of the point - mean) / standard deviation).

Then, the probability of a point that belongs to the distribution would lie within ±t standard deviations from the mean using the probability distribution notes.

The alpha value describes the probability of a point lying outside the range ±t standard deviations from the mean. This is calculated by subtracting the probability by the total area of the probability density curve, which is 1.

Table 3: Used an hypothesis test to verify that the points with highest flux were outliers

Outliers	Point flux value (rounded to 3 decimals)	Mean (rounded to 3 decimals)	Sample Standard Deviation† (rounded to 3 decimals)	Value of t (rounded to 3 decimals)	Value of P††	Value of alpha
Point with highest flux	0.309	0.212	0.016	6.154	1.00	0.00

Point with 2nd highest flux	0.287	0.211	0.013	5.734	1.00	0.00

† For the first outlier (point with the highest flux), the sample was all of the data points. For the second outlier (point with the second highest flux), the sample was all of the data points except the first outlier, which got rejected.

†† Probability of a point that belongs to the distribution would lie within ±t standard deviations from the mean

For both points, the results show alpha to be less than 0.05. According to Chauvenet's Criterion, this shows that the rejection is viable. Therefore, they were discarded for the rest of the analysis. After filtering out these two data points, the relative flux of WASP-2 was plotted for the remaining points in the observation period as shown in Figure 11.

Figure 11: Relative flux of WASP-2 with no outliers The plot has a minimum flux at around 02:00 UTC.

As shown in Figure 12, the stars appear clear at the beginning of the night, but get dimmer towards the end of the night.

a) Processed Image at Start of the Night b) Processed Image at the End of the Night

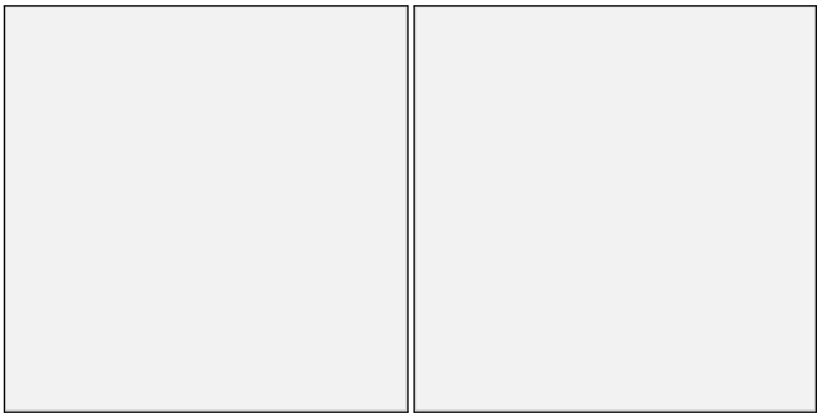

Figure 12: Processed images at the beginning and end of the night. At the beginning of the night, the stars can be clearly seen as shown in part (a). As the night got progressively cloudy, stars started to fade away as shown as (d) In both images, the target star is circled in blue.

This trend can be seen in the graph for the relative flux of WASP-2. Figure 13 shows that the noise increases after two hours from midnight [UTC].

The data were then separated into usable data and unusable data based on the calculated signal-to noise-ratio (SNR) and the minimum SNR needed to detect its transit based on its predicted depth. The separation point was picked because the predicted depth (Jensen E. L. N. 2013) = 91.6 ppt (parts per thousand). For good detection of the transit, the noise needs to be less than the transit depth. If the signal is taken as 1, the signal to noise ratio (SNR) needs to be at least 1/0.0916 or about 10.9. In order for the detection of the transit to be at a 3 sigma level, corresponding to 99% confidence, the usable parts of the data need to have a SNR of at least 32.8. The mean SNR of 5 points directly before the first unusable point is 34.565. The mean SNR of 5 points directly after the first unusable point is 25.989.

Figure 13: Relative flux of WASP-2 divided into an usable part, with low noise levels, and an unusable part, with high noise levels. The means for the first and last portion of the data are similar. However, the standard deviation starts to increase after 02:08 UTC. This indicates that the data were corrupted due to clouds in the atmosphere.

The relative flux of comparison stars was analyzed to confirm that the scattering of the signal during the second half of the data was due to clouds. The SNR for the relative flux of C3 starts to decrease at a similar time as the data from WASP-2, as shown in Figure 14. The mean stays fairly constant throughout the observation period, however the standard deviation starts to increase after 02:00 UTC. This is evidence that the scattering was due to clouds, instead of anything related to the transit.

Figure 14: Initial Relative flux of C3. The mean stays fairly constant throughout the observation period, however the standard deviation starts to increase after 02:00 UTC.

Comparison stars, like C3, show evidence that the noise level starts to increase after approximately 2 hours after the data capture starts, similar to WASP–2b.

Data Split for Transit

The data were split into the pre-transit section, during transit section, and post-transit section, according to the predicted time of transit, which goes from 01:11 UTC to 02:41 UTC (Jensen E. L. N. 2013). Further, a dashed red line was drawn to show the point where the data becomes unusable.

Figure 15: Relative flux of WASP-2 split according to predicted transit time. The difference between the pre-transit/during-transit and post-transit.The red line shows the divide between the usable and unusable data. Note that the SNR of the data starts to decrease in the middle of the transit and becomes progressively worse after the transit. This means that it would be hard to detect the egress of WASP-2b.

To determine the transit depth, the mean of the pre-transit and during transit data were calculated and plotted in Figure 16, along with the standard deviation of the mean for each section. The depth was calculated as per the formula in Equation 2, which is written as

Equation 2: depth = 1 - (mean_during / mean_pre),

where mean_during is the mean for the data taken during the predicted transit, and mean_pre is the mean for the data taken before the transit.